BJRS
BRAZILIAN JOURNAL OF RADIATION SCIENCES

doi.org/10.15392/2319-0612.2024.2695
2024, 12(4A) | 01-21 | e2695
Submitted: 2024-08-30
Accepted: 2025-06-30

Characterization of iron oxide nanoparticles for production of breast adenocarcinoma spheroids

Lima [a*], M. M. P.; Silva [a*], G.D.; Falcão [a*], P. L.; Silva [a*], T. M.; Oliveira [a*], R. R.; Vieira [a*], D. P.;

[a] Instituto de Pesquisas Energéticas e Nucleares, 05508-000, São Paulo, Brazil.

*Correspondence: pazmayelle@gmail.com

Abstract: The construction of an in vitro model that can accurately demonstrate the conditions found in vivo requires the production of a series of complexities that often transcend various areas of knowledge. In this context, the present study employed three-dimensional culture by magnetic aggregation to build a model that minimally satisfactorily represented conditions for studying cellular behaviors present in the tumor environment related to cell death and duplication. Thus, functionalized iron oxide nanoparticles were used for culturing tumor spheroids containing breast adenocarcinoma cell line (MCF7) and human fibroblast (HF002-J) within their structure. The spheroids were divided into concentration categories for each cell line, and after a screening process, the concentrations with greater stability were irradiated or received doses of a drug with known antitumor activity for treatment. The models were studied through X-ray diffraction (XRD), Transmission electron microscopy (TEM), cytotoxicity assays, and fluorescence microscopy. The obtained results proved to be a viable alternative for the analysis of cell viability, cytotoxicity, and the morphology of tumor spheroids.

Keywords: Three-Dimensional Culture, Cancer, Iron Nanoparticles, Cytotoxicity.

SBPR

OPEN ACCESS
CC BY

BJRS
BRAZILIAN JOURNAL OF RADIATION SCIENCES

doi.org/10.15392/2319-0612.2024.2695
2024, 12(4A) | 01-21 | e2695
Submitted: 2024-08-30
Accepted: 2025-06-30

Caracterização de nanopartículas de óxido de ferro para produção de esferoides de adenocarcinoma mamário

Resumo: A construção de um modelo in vitro que possa demonstrar com precisão as condições encontradas in vivo exige a produção de uma série de complexidades que muitas vezes transcendem várias áreas do conhecimento. Nesse contexto, o presente estudo utilizou a cultura tridimensional por agregação magnética para construir um modelo que representasse, de maneira minimamente satisfatória, as condições para o estudo de comportamentos celulares presentes no ambiente tumoral relacionados à morte e à duplicação celular. Assim, nanopartículas de óxido de ferro funcionalizadas foram usadas para cultivar esferoides tumorais contendo linhagens celulares de adenocarcinoma mamário (MCF7) e fibroblastos humanos (HF002-J) em sua estrutura. Os esferoides foram divididos em categorias de concentração para cada linhagem celular, e, após um processo de triagem, as concentrações com maior estabilidade foram irradiadas ou receberam doses de um fármaco com conhecida atividade antitumoral para tratamento. Os modelos foram estudados por meio de difração de raios-X (DRX), microscopia eletrônica de transmissão (TEM), ensaios de citotoxicidade e microscopia de fluorescência. Os resultados obtidos mostraram ser uma alternativa viável para análises de viabilidade celular, citotoxicidade e morfologia de esferoides tumorais.

Palavras-chave: Cultura Tridimensional, Câncer, Nanoparticulas de Ferro, Citotoxicidade.

SBPR

OPEN ACCESS
CC BY

1. INTRODUCTION

The personalized treatment of breast cancer has been extensively studied for the past two decades, focusing on tumor profiling and identifying therapeutic targets and biomarkers for prognosis [1,2]. Tumor development involves complex interactions within the microenvironment, influencing cellular behavior in response to treatments [3].

Multicellular tumor spheroid models offer a platform for studying tumor processes efficiently, with exponential volume growth facilitating high-throughput screening. Magnetite nanoparticles (PIONS) are used for their magnetic properties, allowing directional attraction under a magnetic field while remaining inert without inherent magnetism [5,6].

In this study, PIONS were utilized in a magnetic aggregation/levitation system to create a three-dimensional cell culture model of breast adenocarcinoma. This model maintains cell-to-cell contact, mimicking the tumor microenvironment in vivo. The objective is to assess the effects of ionizing radiation and drug action on breast adenocarcinoma cell spheroids in terms of cell mortality and compare these effects with two-dimensional cultures [7,8].

Multicellular tumor spheroid models mimic functions by sustaining heterogeneous development, enabling efficient studies of specific tumor processes. Additionally, the growth pattern of multicellular spheroid, when compared to solid tumors, exhibits an exponential volume increase on a microscopic scale <500 μm in diameter, facilitating high-throughput automated screening systems [4].

Magnetite (Fe_3O_4) is a paramagnetic iron oxide composed of ferrous ions (Fe^{+2}) and ferric ions (Fe^{+3}) distributed in different crystallographic sites. The crystalline structure of

this material can be described as an inverse spinel, and the generated particles are mostly cubic, dark, easily manipulated, and highly functionalizable for various applications [5,6].

2. MATERIALS AND METHODS

2.1. Cell Culture

A human breast adenocarcinoma cell line, MCF7 (ATCC® HTB-22™), was maintained in 25 cm^2 culture bottles containing RPMI-1640 medium (Gibco), supplemented with 10% (v/v) fetal bovine serum and 5% antibiotic solution (10,000 IU/mL penicillin, 10 mg/mL streptomycin, and 1 mg/mL amphotericin), in a controlled, humidified atmosphere with 5% CO_2 at 37°C.

2.2. Synthesis of iron nanoparticles

A synthesis of PIONS was conducted through co-precipitation of iron hydroxides using a microwave-assisted synthesis approach. Initially, 32.5 mM of $FeSO_4 . 7H_2O$ (Sigma-Aldrich®) and 92.4 mM of $C_2H_5NO_2$ (Sigma-Aldrich®) were dissolved in a beaker containing 80 mL of deionized water under constant stirring to achieve a homogeneous solution. Subsequently, a 2 molar NaOH solution was slowly dropwise added into the mixture under continuous stirring until the pH reached 6.5. After irradiation at 950 W for 2 minutes and 30 seconds, a black precipitate was formed. The precipitate was separated, washed with deionized water, and treated with acetic acid. A solution containing $((C_6H_{14}N_2O_2)_n)$ was then added dropwise under ultrasonic conditions. The product was resuspended in ultrapure water for storage.

2.3. X-Ray Diffraction (XRD) and Transmission Electron Microscopy (TEM)

Stored in a microtube, 500 μL of the sterile PIONS suspension were withdrawn. With the aid of a magnet, as much liquid as possible was removed from the magnetic precipitate and subsequently washed with 1000 μL of ethyl alcohol (Alphatec). After discarding the alcohol, the microtube remained open inside a beaker in the drying oven for a period of 24 hours at 42ºC for total evaporation of the liquids present in the sample. The X-ray diffraction patterns of the powdered sample were characterized using the Rigaku diffractometer, model DMAX 2100, with CuKα radiation (λ = 1.15416 Å) accelerated by a potential of 40 kV at a current of 20 mA. The QualX2 software was used to analyze the obtained XRD patterns, employing data comparison from COD (Crystallography Open Database) where the peak distances maintain the characteristic of the crystalline phase being observed. The powder sample of PIONS was analyzed using a high-resolution JEM-2100 microscope (JEOL) operated at 200 kV. The application of this method was associated with observing the morphology and dispersion of the NPs. The sample was dispersed in 1 mL of isopropyl alcohol, placed on a copper grid covered with a flat carbon film, and analyzed under bright-field conditions.

2.4. Adsorption of magnetite nanoparticles on the surface of cells and spheroid formation

The PIONS were added at a ratio of 2 μL (approximately 3 mM of iron) for every 1.5x106 suspended cells. The cell-nanoparticle suspension was homogenized by pipetting and added to a 25 cm^2 culture bottle, then maintained in culture overnight at 37ºC with 5% CO_2. Cell culture plates with 96 wells were pre-treated with a solution of Pluronic® F-127 (0.5 g/L in 2-propanol, Sigma-Aldrich). This solution was heated at 60ºC for 10 minutes or until the viscosity was completely reduced, as evidenced by the absence of turbidity in the solution. Volumes of 150 μL/well were transferred to the plates. The treated plates were

sealed (Parafilm®) and left at room temperature for 24 hours within the laminar flow hood to maintain sterility. After this period, the liquid was removed from the wells by suction using a vacuum pump, and the plates remained open within the sterile laminar flow hood for drying under UV radiation for 30 minutes.

2.5. Irradiation

For plate preparation prior to irradiation, as much culture medium as possible was removed from the 96-well culture plates, and 10 µL/well of PBS at room temperature was added. After 10 minutes, the plates were irradiated with doses of 0.5, 2, and 4 Gy using a ^{60}Co gamma radiation source (GammaCell) at the Radiation Technology Center (CETER – IPEN), at a dose rate of 130 kGy/h. Following irradiation, the plates were washed with PBS, 100 µL/well of RPMI-1640 medium (Gibco) was added, and they were placed in the incubator at 37ºC and 5% CO2, where they remained for 4-8 days until analysis using the INCell Analyzer 2500 HS (Cytiva Lifesciences) op-tical microscope located at the CEBIO building, IPEN – CNEN.

2.6. Fluorescence Microscopy Assays

The plates were stained with SYTOX® Green (10 µL/well, Thermo Scientific) and Hoechst 33342 (10 µg/mL, Sigma-Aldrich) in culture medium and kept in the incubator for 60 minutes for analysis. The SYTOX® Green dye stains the nuclei of all non-viable cells present in the sample, while the Hoechst 33342 dye stains all nuclei. The experiments were monitored at intervals of four days for irradiated samples and eight days for non-irradiated sample screenings. The experiments were conducted using the INCell Analyzer 2500 HS equipment (Cytiva Lifesciences), employing a 4X objective lens (Nikon 4X/o.20, Plan Apo, CFI/60) and acquiring images in brightfield (clear field), blue (Hoechst 33342 fluorescence), and green (SYTOX® Green fluorescence) channels. Each spheroid was captured in stacks

comprising 30 to 100 planes (slices) spaced by 3 to 15 μm (z). Analyses were carried out using the INCarta 1.12 software (Cytiva Lifesciences).

2.7. Cytotoxicity assays

Cell viability studies were performed using Cell-Repellent 96-well plates (Greiner BIO-ONE). Cells were seeded at $5x10^3$ cells/well (60 μL/well) using the magnet-coupled plate on the Cell-Repellent plate. After 24 hours of incubation at 37ºC and 5% CO_2, the treatment stage was carried out using Mitomycin-C drug and control groups, where each well of the 96-well plate received 20 μL of the desired solution for analysis. For this assay, Dimethyl sulfoxide (DMSO) and Sodium Dodecyl Sulfate (SDS) were used as positive control groups; Sodium Chloride (0.045%) as the negative control, and the Mitomycin-C drug at different concentrations (1.56; 0.75; 0.375; 0.1875; 0.093 and 0.048 μg/mL). After 24 hours of application, the plate was treated with MTS solution (CellTiter 96® AQueous Non-Radioactive Cell Proliferation Assay (MTS), Promega®) and PMS (Phenazine methosulfate, Sigma-Aldrich), 40 μL/well, and returned to the incubator for an additional 2 hours until the absorbance (490 nm) was read using the Multiskan EX plate spectrophotometer (Thermo) located in the CEBIO building, IPEN – CNEN.

3. RESULTS AND DISCUSSIONS

The analysis of the PIONS used for constructing the 3D cell culture model prioritized the morphology and size of the synthesized particles. Figure 1 illustrates the X-ray pattern obtained from the sample analyzed by XRD. The diffractogram indicates diffraction peaks attributed to the inverted spinel structure corresponding to the crystalline arrangement of magnetite (Fe_3O_4, COD: 00-153-2800). The average sizes of the crystallites obtained were calculated to be 57.574 nm using the Scherrer equation.

The TEM images effectively illustrate the distribution and shape of Fe_3O_4 nanoparticles, displaying quasi-cubic particles. A considerable size distribution was observed in the studied sample, as shown in Figure 2. Atomic planes are visible in some nanoparticles, highlighting the monocrystalline characteristics present in the sample. The interaction of the high-energy electron beam with the sample reveals PIONS with minimal aggregation artifacts, observed at spatial resolutions of 5 nm and 20 nm.

Figure 1: X-ray diffractogram of the sample of iron oxide nanoparticles synthesized with Glycine (Gly) as a surfactant and functionalized with Poly-L-lysine (PLL). The numbers above the peaks refer to the crystalline planes found in the samples

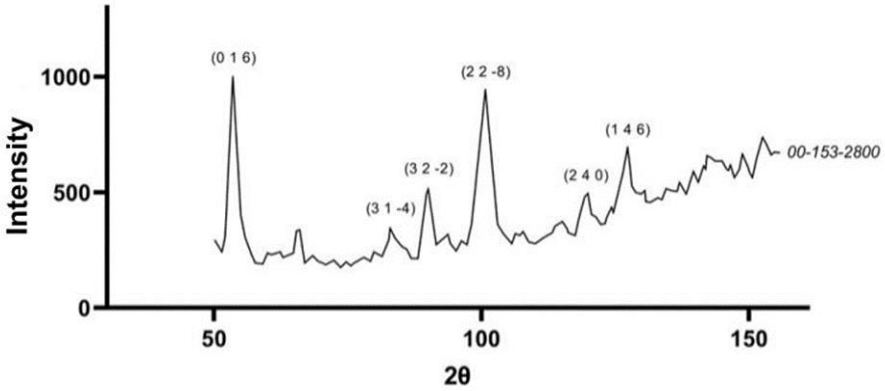

Source: Created by the author.

Figure 2: Transmission Electron Microscopy (TEM) images of iron oxide nanoparticles synthesized with Glycine (Gly) as a surfactant and functionalized with Poly-L-lysine (PLL).

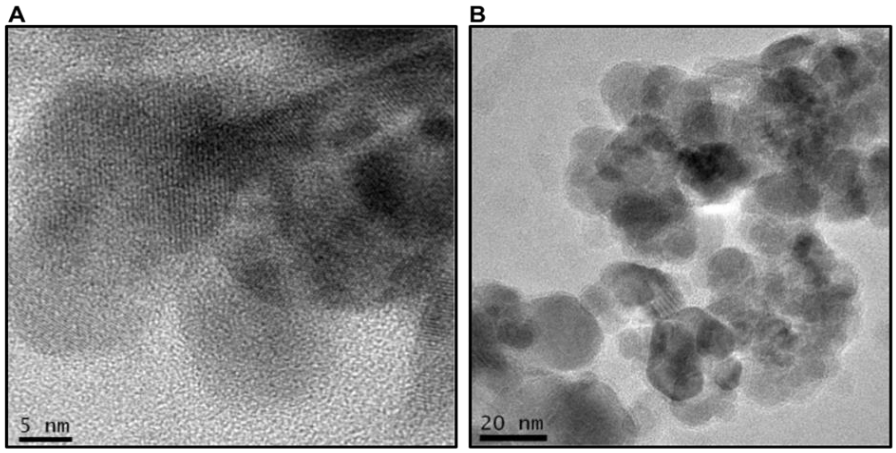

Source: Created by the author.

The stability of Fe_3O_4 NPs and their biocompatibility with PLL functionalization have been previously investigated by the group [10]. Thus, in the current work, the NPs were synthesized to serve as the basis for constructing the 3D cell culture model. The use of these NPs in cell cultures resulted in outcomes consistent with expectations, maintaining strong adhesion to the cell membrane and resistance to subsequent trypsinization/manipulation assays.

For the construction of the 3D model, biomedical and biocompatible polymers such as Pluronic® F-127 were studied. These polymers have been used as drug carriers in medicine due to their ability to form micelles—amphiphilic structures that separate the internal and external environments in which the structure is aggregated [11]. In this work, Pluronic® F-127 in anhydrous 2-propanol was used, allowing the hydrophobic portion of the micelle to be directed towards the center of the well, preventing cellular adhesion.

Figure 3 depicts the typical appearance of MCF7 spheroids after 24, 48, or 72 hours of incubation. In this experiment, the stability of spheroids after hours of incubation was assessed based on the amount of SYTOX® Green-positive cells, indicating cell death. The acquisitions reveal a reduction in the number of dead cells after 72 hours of incubation, indicating an overall increase in the total number of cells and a relative decrease in the concentration of non-viable cells over the incubation period. The experiment demonstrated that spheroids incubated for 72 hours remained intact, exhibited low friability (fewer fragments), and had few events of cell death, making them suitable for experiments.

The treatment model for 96-well plates, as explained throughout this study, remains a viable option for the cultivation and analysis of MCF7 spheroids using the INCell Analyzer 2500 HS fluorescence microscopy equipment (Cytiva Lifesciences). The Figure 4 depicts the quantification of dead cell nuclei (A) and spheroid volume (B) irradiated at 2 Gy in plates treated with Pluronic® F-127. Plates treated in this manner exhibited good compatibility with fluorescence microscopy studies. However, when used for cytotoxicity assays, this

technique did not provide reproducibility in terms of absorbance values. Therefore, this study maintained the use of Cell-Repellent 96-well plates (Greiner BIO-ONE) to enhance the technique used in subsequent assays.

Figure 3: Evaluation of spheroid growth. Photomicrographs obtained by fluorescence microscopy using the INCell Analyzer 2500 HS (Cytiva Lifesciences) over eight days in a 96-well plate with SYTOX® Green (green) indicating dead cell nuclei and Hoechst 33342 (blue) indicating viable nuclei. Scale bar of 200 μm.

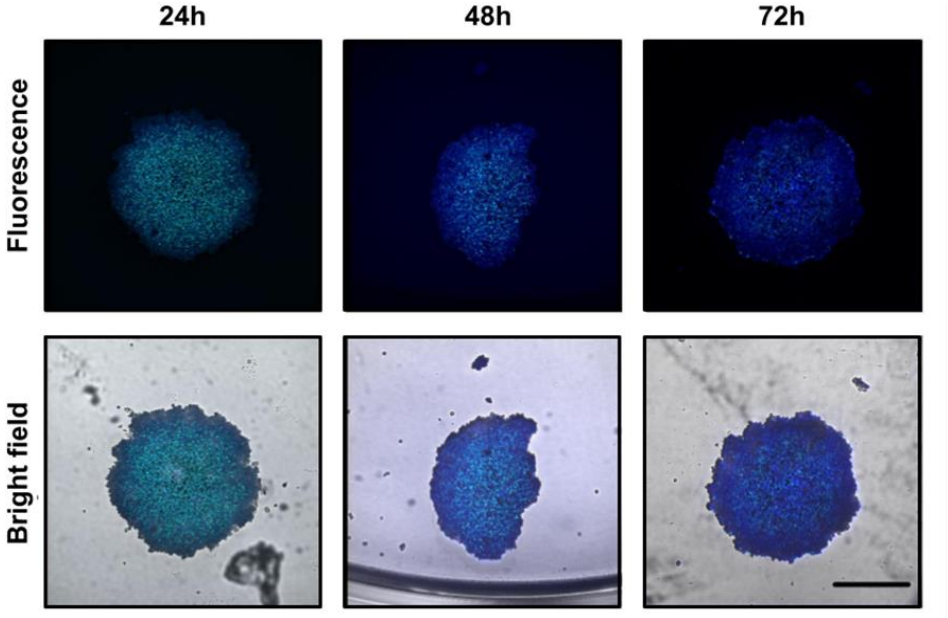

Source: Created by the author.

Figure 4: Quantities of dead cells (A) and spheroid volumes (B) of MCF7 irradiated at 2Gy. Bars represent standard errors of the means. (*): p <0.05. (**): p <0.001. (****): p <0.0001. (ns): not significant compared to control (24h).

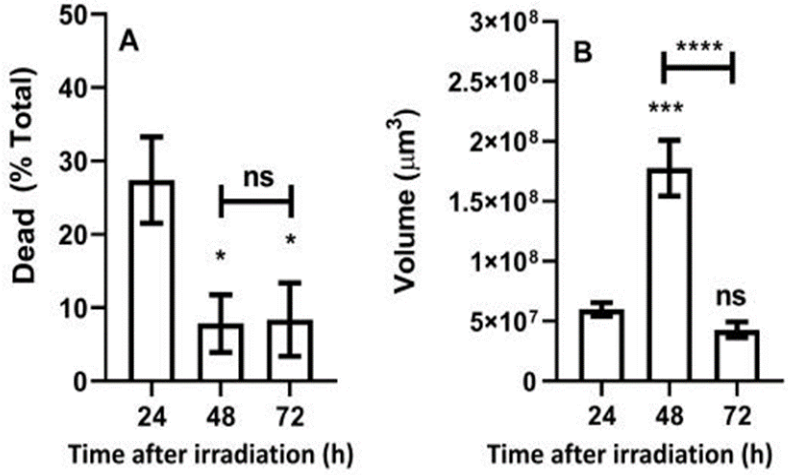

Source: Created by the author.

The cell viability control depicted in Figure 5 utilizes the quantitative colorimetric assay principle to measure the cells' metabolic activity. The reduction of the tetrazolium compound (MTS) uses the phenazine-based reagent Phenazine Methosulfate (PMS) in culture medium for mitochondrial reductase reaction [12,13]. As observed, the positive control group composed of Dimethyl Sulfoxide (DMSO), a universal solvent for both polar and nonpolar compounds, exhibited cytotoxicity gradually concerning the percentage amount added to the culture. This outcome aligns with findings in the literature [14]. The positive control group using Sodium Dodecyl Sulfate (SDS) induced a different response. Apparently, the denaturant acted upon the cells, inducing cytotoxicity at higher amounts in various concentrations, showing relevant toxicity from 625 μM onward, as depicted in Figure 5.

Figure 5: Cytotoxicity of SDS concentrations in MCF7 spheroids. Bars: standard error of the means. (****): p <0.0001. Statistical significance measured concerning the control group (CC).

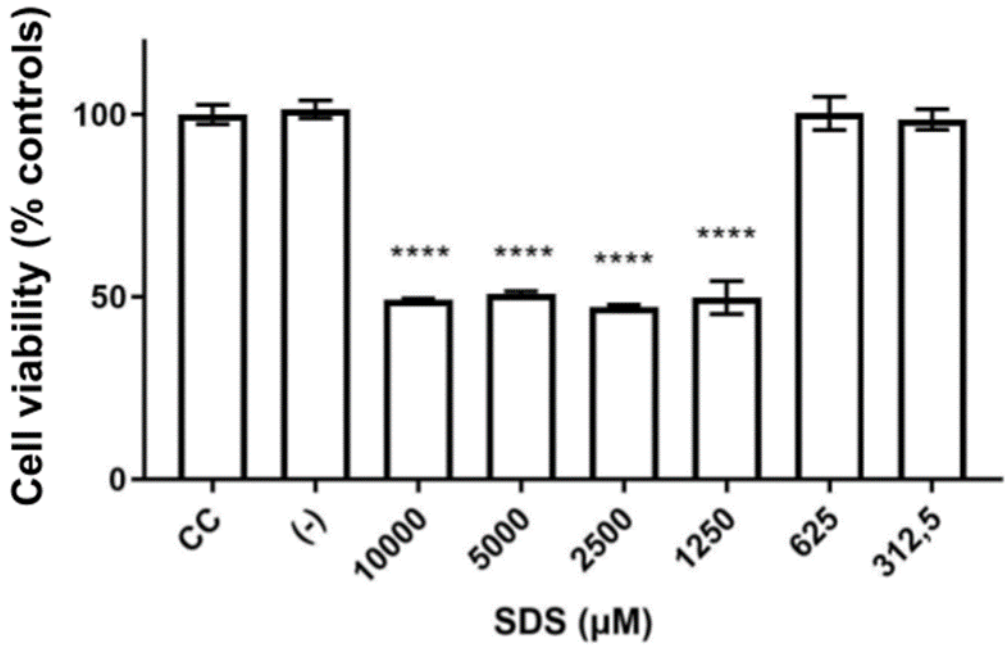

Source: Created by the author.

Mitomycin-C has a discreet antitumor action in MCF7 2D cultures [15,16,17]. However, reports indicate its difficulty in diffusion within solid tumors, requiring artificial perfusion or vascularization in in vivo settings [18], suggesting challenges in penetrating

various cell layers. The three-dimensional structure allows the emergence of nutrient, waste, gas, and pH gradients across cellular layers. The pH value decreases as it penetrates the layers [19]. Mitomycin-C degrades in low pH [20], and its relatively low diffusion capacity, possibly coupled with its pH sensitivity, aligns with the reduced efficacy reported in this study, as depicted in Figure 6 (A).

Literature associates DMSO with an apparently bimodal effect; at low doses, DMSO might even be considered beneficial for cells, but at higher concentrations, this agent tends to be extremely toxic due to its ability to mediate cell death through apoptosis and necrosis [21]. In Figure 6 (B) demonstrates that percentages of 20% and 40% DMSO can be used as a positive control for cytotoxicity testing in MCF7 cells maintained in three-dimensional culture.

Figure 6: Cytotoxicity of MTMC concentrations in MCF7 spheroids (A). Bars: standard error of the mean. (****): p <0.0001. Cytotoxicity of DMSO concentrations in MCF7 spheroids (B). Bars: standard error of the mean. (****): p <0.0001. (*): p <0.05. C. Statistical significance related to the control group (CC).

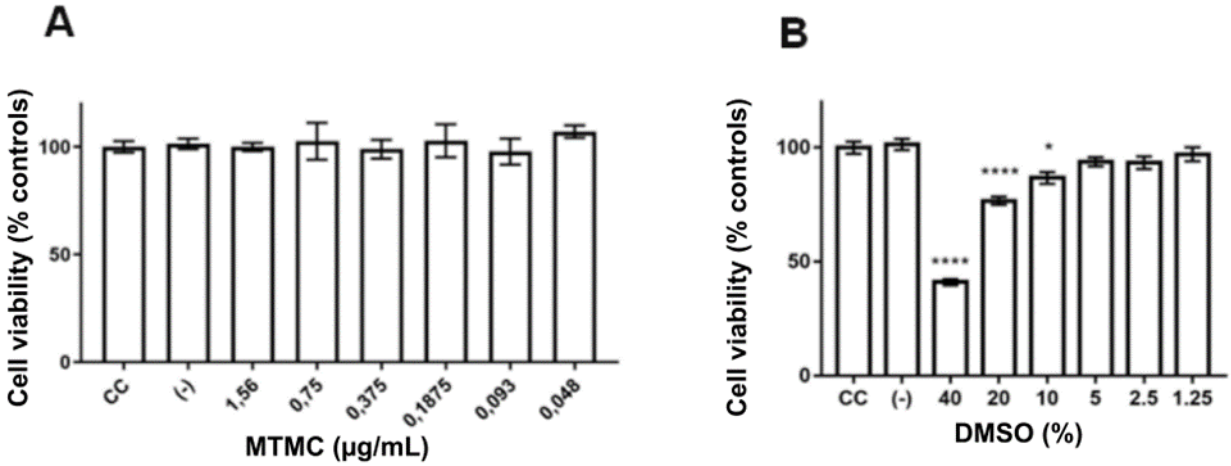

Source: Created by the author.

Figure 7 depicts the typical appearance of spheroids composed of 60% MCF7 and 40% HF002-J concentration after 24 hours of incubation, analyzed over eight days post-seeding. It was possible to observe an increase in the spheroid diameter over the culture period. Differences were noted between the numbers of dead cells, stained green with SYTOX® Green, and the number of intact nuclei, stained blue with Hoechst 33342. On the

first day, only a few areas within the spheroid showed cell death, while by the eighth day, a considerable area in the interior tested positive for cell death.

Figure 7: Evaluation of spheroid growth. Photomicrographs obtained by fluorescence microscopy using the INCell Analyzer 2500 HS equipment (Cytiva Lifesciences) for eight days (1, 2, 3, 4, 5, 6, 7, and 8) in a 96-well plate with SYTOX® Green (green) indicating dead cell nuclei and Hoechst 33342 (blue) indicating viable nuclei. Scale bar: 200 μm.

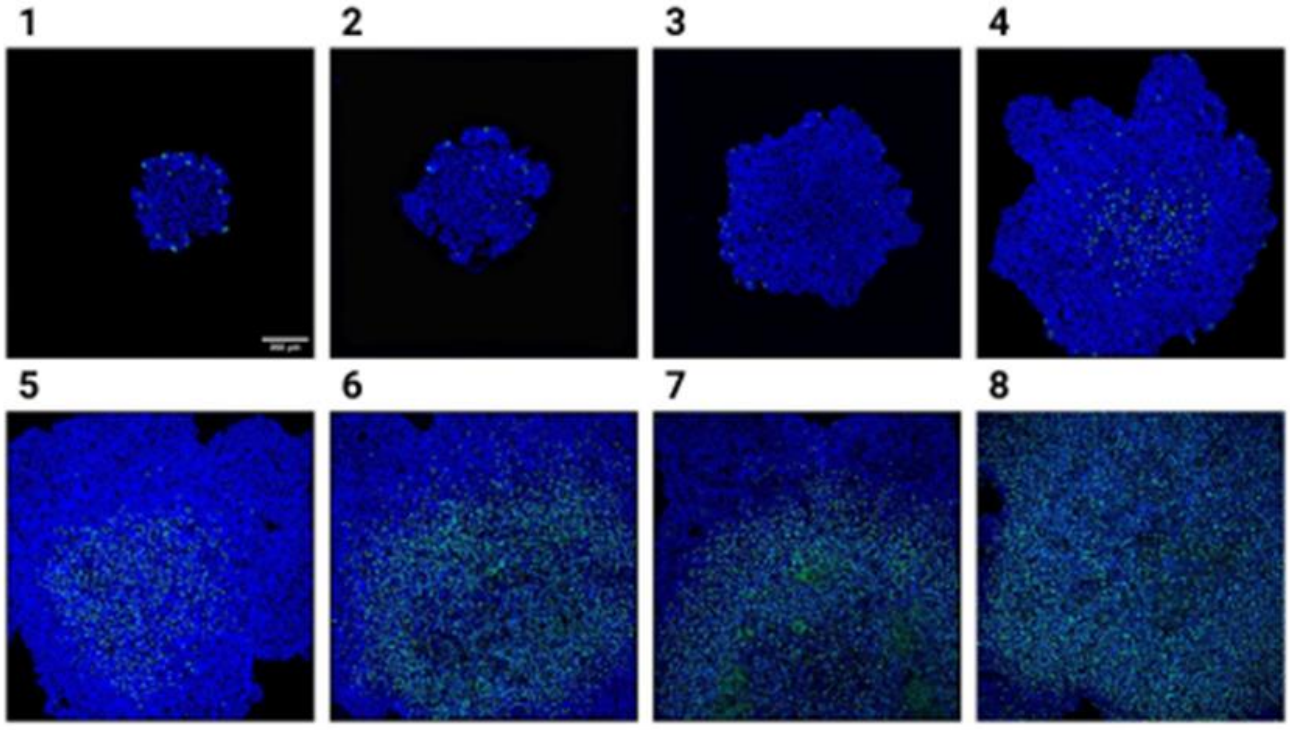

Source: Created by the author.

From the obtained images, a pattern of increased mortality among the various combinations of studied lineage concentrations over the culture days was analyzed, as observed in Figure 8. It is possible to infer that from the fourth day onwards, the amount of cell death increases considerably; the spheroids were maintained for eight days without changing the culture medium. At the periphery of the spheroid, mostly viable cells are found, while in the center of the three-dimensional structure, non-viable cells are found, possibly due to the difficulty of nutrient and oxygen diffusion to the center and of excreta and CO_2 to the outer medium due to the more pronounced cell-to-cell interaction in this type of culture [22]. Due

to the lack of nutrients in the medium, the cells present in the spheroids, in most of the concentrations used, exceeded 50% mortality in the total cells studied.

Figure 8: Graph of mortality percentages (non-viable nuclei, positive for SYTOX® Green) in spheroids formed by different ratios of MCF7 and HF002-J over the course of the experiment days. Concentrations referring to the MCF7/HF002-J fraction.

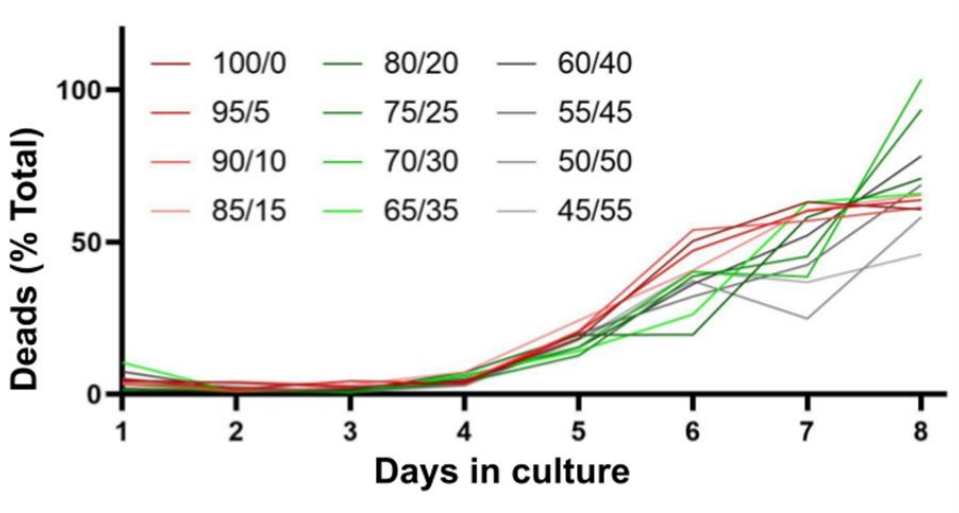

Source: Created by the author.

Throughout the experiment, the field of view captured by the 4X objective appeared to be insufficient for the dimensions of the sample due to the increased volume of the spheroid. Until the fifth day, the sample could be analyzed integrally within the equipment's field of view, but from the sixth day onwards, only about half of the extension of each sample could be analyzed, and by the eighth day, only about a third corresponded to the analyzed field of view. This variation can be observed in Figure 9. The volumes of the spheroids in the plate showed a gradual growth until the fifth day, a phenomenon already predicted in the literature related to the normalized growth of seeded cells [23]. With the restricted field of view, the analyses began to deviate in counting, leading to a considerable reduction between the computed volumes.

When analyzing a co-culture spheroid, it should be taken into consideration that besides the differences between the studied cell lines, the size and geometry of the spheroid corroborate with the characteristics present in the studied microenvironment. It is common for central cells to

tend to be smaller due to compression by cell-cell interaction, while peripheral cells maintain a larger size due to the high rate of cell proliferation in this area [24,25].

Figure 9: Spheroid volumes as a function of days in culture. Concentrations corresponding to the MCF7/HF002-J fraction.

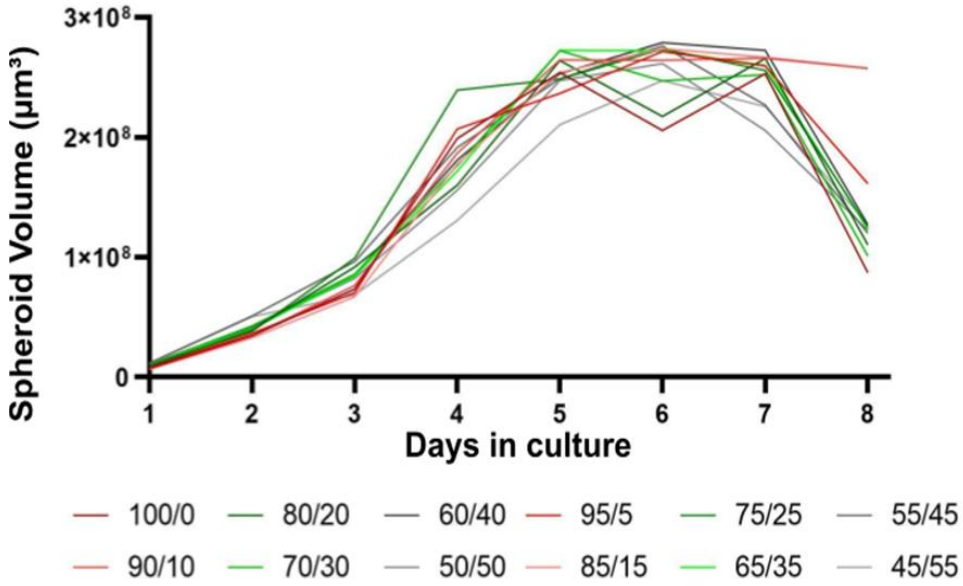

Source: Created by the author.

The control of the total cell volume, as observed in Figure 10, demonstrates that in the initial days of culture, cells are adapting to the site where they were seeded. Over the course of days, the spheroid undergoes a more pronounced variation in nuclear volume, and this phenomenon occurs heterogeneously among the studied concentrations.

When we observe the volumetric difference between the nuclei of non-viable cells, as shown in Figure 11, we see expectedly reduced sizes that undergo significant changes over time when compared to the same sampling populations. It can also be noted from this result that starting from the third day, nuclei begin to exhibit statistical differences, which may involve the increasing amount of mortality during this same studied period.

The variation in nucleus volume occurs due to factors that are related and may be linked to different categories such as cell type, cell cycle, temperature, pH present within nuclear organelles, and among other aspects that are still being studied for a better definition of this

morphological characteristic [26,27,28]. It can be influenced by the activity of proteins of the nuclear envelope, especially laminins forming the protein scaffolds of the nuclear envelope [29] and by other proteins such as nesprins, which connect the nuclear envelope to the cytoskeleton and are related to cell cycle processes [30].

Nuclear mechanics, described over the years, is based on chromatin dispersion, responsible for organizing the macromolecules present in the nucleus, and surface rigidity, directly impacting the size and shape of the nucleus [31,32].

Figure 10: Control charts of total nucleus volume as a function of days in culture. Concentrations corresponding to the MCF7/HF002-J fraction. Bars: standard errors of the means. (*) p <0.05. (**) p <0.01. (***) p <0.001. (****) p <0.0001 relative to control (Day 1).

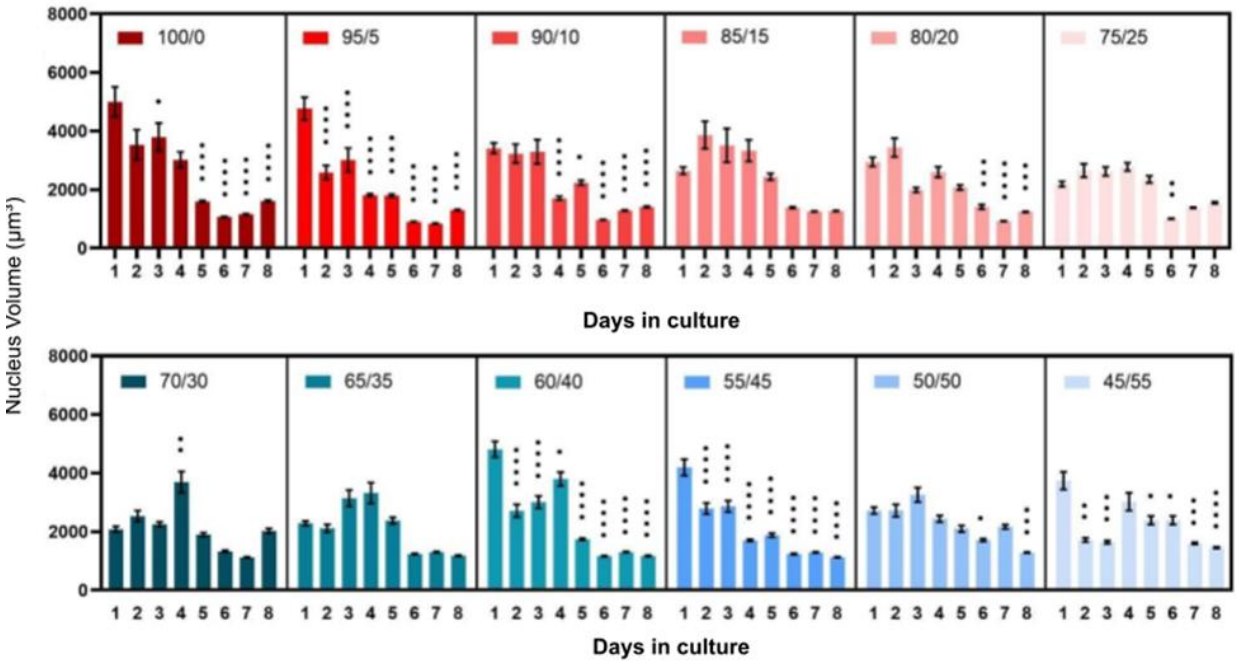

Source: Created by the author.

Figure 11: Control charts of volume of nuclei of non-viable cells over the days in culture. Concentrations referring to the MCF7/HF002-J fraction. Bars: standard errors of the means. (*): p <0.05. (**): p <0.01. (***): p <0.001. (****): p <0.0001 compared to control (Day 1).

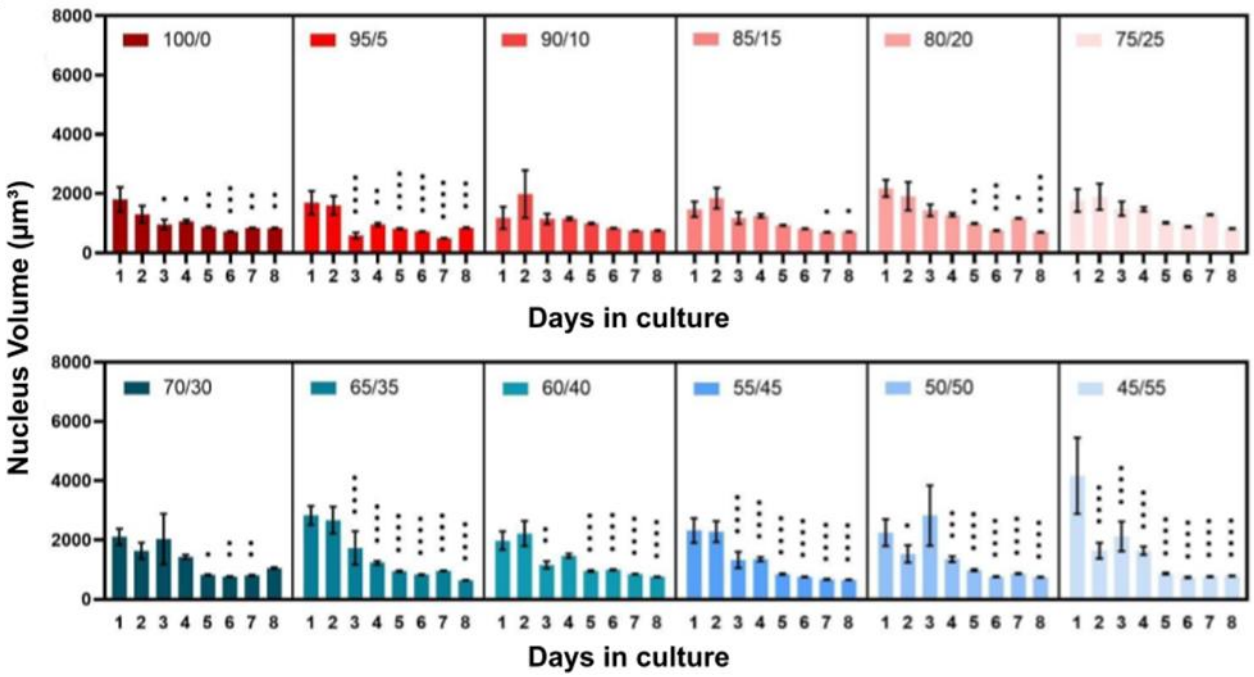

Source: Created by the author.

4. CONCLUSIONS

The biocompatible model of three-dimensional culture, constructed through magnetic levitation as presented in this study, proved to be a viable alternative for analyzing cell viability, cytotoxicity, and morphology of a tumor spheroid. Based on the results obtained, it was possible to conclude that mitomycin C is not a favorable drug for the treatment of breast tumors, as it requires high doses to have an effect on the tissue, potentially leading to significant side effects with the use of this therapy.

ACKNOWLEDGMENT

The authors would like to thank Eng. Elizabeth Somessari for technical advisement during the irradiation experiments, as well as the Centro de Tecnologia das Radiações (CETER) at IPEN for providing the infrastructure and support necessary for the irradiation procedures.

FUNDING

The authors also acknowledge the financial support from the National Nuclear Energy Commission (CNEN), through a research scholarship (Process No. 01341001294/2021-21), and from the Financier of Studies and Projects (FINEP), under process number:01.18.0073.00 - Implementation of mobile facilities to make the technology generated available to the productive sector and society.

CONFLICT OF INTEREST

All authors declare that they have no conflicts of interest.

REFERENCES

[1] MARCOM, P.K. Chapter 10 - Breast Cancer. Genomic and Precision Medicine (Third Edition), pp.181-194, 2017.

[2] HERIOT, A. G. 7 - Personalized Cancer Care. Perioperative Care of the Cancer Patient, pp. 83-90, 2023.

[3] ZANONI, M. et al. Modeling neoplastic disease with spheroids and organoids. Journal of Hematology & Oncology, v. 13, 2020.

[4] KHANNA, S. et al. Chapter 13 - Multicellular tumor spheroids as in vitro models for studying tumor responses to anticancer therapies. Animal Biotechnology (Second Edition), pp. 251-268, 2020.

[5] DUTTA, S. et al. Chapter 7 - Remediation of heavy metals with nanomaterials. Separation Science and Technology, v. 15, pp. 97-138, 2022.

[6] LAMICHHANE, N. et al. Chapter 13 - Superparamagnetic iron oxide nanoparticles (SPIONs) as therapeutic and diagnostic agents. Nanoparticle Therapeutics, pp. 455-497, 2022.

[7] TIWARI, A. K. et al. Chapter 10 - Magnetic nanoparticles: challenges and practical considerations. Multifunctional Nanocarriers, pp. 235-257, 2022.

[8] BRAIM, F. S. et al. Rapid green-assisted synthesis and functionalization of superparamagnetic magnetite nanoparticles using Sumac extract and assessment of their cellular toxicity, uptake, and anti-metastasis property. Ceramics International, v. 49, pp. 7359-7369, 2023.

[9] EKE, G. et al. Cell Aggregate Assembly through Microengineering for Functional Tissue Emergence. Cells, v. 11, 2022.

[10] BONFIM, L. et al. Microwave-mediated synthesis of iron-oxide nanoparticles for use in magnetic levitation cell cultures. Appl. Nanosci., pp. 1707–1717, 2019.

[11] OTTENBRITE, R. M. ; JAVAN, R. Biological Structures. Encyclopedia of Condensed Matte Physics, pp. 99–108, 2005.

[12] MALICH, G. et al. The sensitivity and specificity of the MTS tetrazolium assay for detecting the in vitro cytotoxicity of 20 chemicals using human cell lines. Toxicology, v. 124, pp. 179-192, 1997.

[13] KUETE, V. et al. Chapter 10 - Anticancer Activities of African Medicinal Spices and Vegetables. Medicinal Spices and Vegetables from Africa, pp. 271-297, 2017.

[14] DLUDLA, P. V. et al. Chapter 25 - The impact of dimethyl sulfoxide on oxidative stress and cytotoxicity in various experimental models. Toxicology, pp. 243-261, 2021.

[15] ZHOU, Q. M. et al. Curcumin reduces mitomycin C resistance in breast cancer stem cells by regulating Bcl-2 family-mediated apoptosis. Cancer Cell International, v. 17, 2017.

[16] AL-OTAIBI, W. A. et al. Cytotoxicity and apoptosis enhancement in breast and cervical cancer cells upon coadministration of mitomycin C and essential oils in nanoemulsion formulations. Biomedicine & Pharmacotherapy, v. 106, pp. 946-955, 2018.

[17] PIMIA, F. et al. Mitomycin C induces apoptosis and caspase-8 and -9 processing through a caspase-3 and Fas-independent pathway. Cell Death & Differentiation, v. 9, pp. 905-914, 2002.

[18] FISCHER, L. M. et al. Exploration of two methods for quantitative Mitomycin C measurement in tumor tissue in vitro and in vivo. Biological Procedures Online, v. 15, 2013.

[19] BOEDTKJER, E ; PEDERSEN, S. F. The Acidic Tumor Microenvironment as a Driver of Cancerm. Annual Review of Physiology, v. 82, pp. 103–126, 2020.

[20] FANG, Y. P. et al. Diminishing the side effect of mitomycin C by using pH-sensitive liposomes: in vitro characterization and in vivo pharmacokinetics. Drug Des Devel Ther, v. 15, pp. 159-169, 2018.

[21] DLUDLA, P. V. et al. A dose-dependent effect of dimethyl sulfoxide on lipid content, cell viability and oxidative stress in 3T3-L1 adipocytes. Toxicology Reports, pp. 1014-1020, 2018.

[22] ZHANG, W. et al. Optimization of the formation of embedded multicellular spheroids of MCF-7 cells: How to reliably produce a biomimetic 3D model. Analytical Biochemistry, v. 515, pp. 47-54, 2016.

[23] JAYME, C. C. et al. DNA polymer films used as drug delivery systems to early-stage diagnose and treatment of breast cancer using 3D tumor spheroids as a model. Photodiagnosis and Photodynamic Therapy, v. 37, 2022.

[24] ROJAS-CALDERÓN, E. K. et al. Monte Carlo calculations of the cellular S-values for α-particle-emitting radionuclides incorporated into the nuclei of cancer cells of the MDA-MB231, MCF7 and PC3 lines. Applied Radiation and Isotopes, v. 135, pp. 1-6, 2018.

[25] BIALKOWSKA, K. et al. Spheroids as a type of three-dimensional cell cultures—examples of methods of preparation and the most important application. International Journal of Molecular Sciences, v. 21, pp. 1-17, 2020.

[26] CHAN, C. J. et al. Volume Transitions of Isolated Cell Nuclei Induced by Rapid Temperature Increase. Biophysical Journal, v.112, pp. 1063-1076, 2017.

[27] CANTWELL. H. ; NURSE, P. Unravelling nuclear size control. Current Genetics, v. 65, pp. 1281–1285, 2019.

[28] EFREMOV, A. K. et al. Nucleus size and its effect on nucleosome stability in living cells. Biophysical Journal, v. 121, pp. 1-16, 2022.

[29] JEVTIC, P. et al. Concentration-dependent Effects of Nuclear Lamins on Nuclear Size in Xenopus and Mammalian Cells. The Journal of Biological Chemistry, v. 290, pp. 27557-27571, 2015.

[30] LU, W. et al. Nesprin interchain associations control nuclear size. Cellular and Molecular Life Sciences, v. 69, pp. 3493−3509, 2012.

[31] LEBEAUPIN, T. et al. 9 - The Multiple Effects of Molecular Crowding in the Cell Nucleus: From Molecular Dynamics to the Regulation of Nuclear Architecture. Nuclear Architecture and Dynamics, pp.209-232, 2018.

[32] BAIRAMUKOV, V. Y. et al. AFM imaging of the transcriptionally active chromatin in mammalian cells' nuclei. Biochimica et Biophysica Acta (BBA) - General Subjects, v. 1866, 2022.

LICENSE

This article is licensed under a Creative Commons Attribution 4.0 International License, which permits use, sharing, adaptation, distribution and reproduction in any medium or format, as long as you give appropriate credit to the original author(s) and the source, provide a link to the Creative Commons license, and indicate if changes were made. The images or other third-party material in this article are included in the article's Creative Commons license, unless indicated otherwise in a credit line to the material.
To view a copy of this license, visit http://creativecommons.org/ licenses/by/4.0/.